Chinese Chemical Letters 34 (2023) 107768

Contents lists available at ScienceDirect

Chinese Chemical Letters

journal homepage: www.elsevier.com/locate/cclet

Ultrasound-induced elevation of interlayer spacing and conductivity of CoNi hydroxides for high-performance Ni–Zn batteries

Hongxuan Tang[a,1], Jiujiu Ge[a,1], Lanze Li[a], Xinqiang Zhu[a], Sai Wu[a], Fan Wang[a], Yajun Pang[a,*], Zhehong Shen[a], Cao Guan[b,**], Hao Chen[a,c,*]

[a] College of Chemistry and Materials Engineering, Zhejiang A&F University, Hangzhou 311300, China
[b] Institute of Flexible Electronics, Northwestern Polytechnical University, Xi'an 710072, China
[c] School of Materials Science and Engineering, Zhejiang University, Hangzhou 310027, China

ARTICLE INFO

Article history:
Received 18 June 2022
Revised 19 July 2022
Accepted 20 August 2022
Available online 23 August 2022

Keywords:
Ni–Zn batteries
Cathodes
Metal hydroxide
Interlayer spacing
Ultrasound-assisted method
Room temperature

ABSTRACT

Nickel–zinc (Ni–Zn) batteries hold a lot of promise for energy storage thanks to their high output voltage, plentiful Zn supply, and low toxicity. Achieving the facile preparation of high-performance cathodes at ambient temperature remains a challenge, it is however essential for practical applications. Here, in the present study, an efficient ultrasound-assisted one-step fabrication of CoNi double hydroxide (UA-CoNi DH) microspheres at room temperature that performs well as a cathode for Ni–Zn batteries was proposed. This designed ultrasound-assisted method induces the formation of metal double hydroxide with an elevation of interlayer spacing and bulk conductivity while maintaining the structure features of CoNi DH prepared without ultrasound assistance. As a result, the UA-CoNi DH as an electrode material displays highly enhanced electrochemical properties relative to CoNi DH prepared without ultrasound assistance. Benefitting from the improved performance of our UA-CoNi DH electrode, the Ni–Zn battery with UA-CoNi DH as the cathode (UA-CoNi DH//Zn) delivers a good specific capacity (202.36 mAh/g) and rate performance (70.49% capacity maintained at a 10-fold higher current), presenting more than 71.61% and 21.99% improvement relative to the CoNi DH//Zn battery, respectively. This work offers guidelines for constructing high-performance Ni–Zn battery cathodes in an open environment.

Global industrial production has considerably improved human living, but it has also brought about increasingly serious energy and environmental crisis [1,2]. The development of advanced green energy conversion and storage technologies has become a higher requirement for the sustainable development of modern society [3,4]. In particular, various energy storage devices have been developed for decades to solve the concerns of energy consumption and environmental pollution [5–10]. Aqueous rechargeable batteries are one of the most attractive alternatives for grid-scale energy storage because of their excellent safety, low cost, and environmental friendliness, benefitting from abundant anodes and water-based electrolytes [11–15]. Among them, alkaline nickel–zinc (Ni–Zn) batteries have garnered intensive research attention due to the advantages of the high output voltage and excellent theoretical specific energy density, making it a new generation of high-efficiency energy storage devices after lithium-ion batteries [16–19]. So far, significant progress has been achieved in promoting the Zn anode utilization and enhancing the specific capacity, its practical application is however still restricted by the rational synthesis of Ni-based cathodes [20,21]. To address this bottleneck, several strategies for designing high-performance cathodes have been reported, including sulfidation, solvothermal ion doping, integrating heterostructure, and designing 3D structures [22–25]. Yet, these most commonly used methods are often complex and/or require harsh reaction conditions, making them difficult to utilize in mass production. Therefore, it is desirable to explore efficient strategies to synthesize active cathodes for Ni–Zn batteries at room temperature in an open environment.

Cobalt–nickel hydroxides have been found to possess better performance than their respective nickel hydroxide and cobalt hydroxide counterparts as cathodes for Ni–Zn batteries because of their ability to produce more active sites and intrinsic synergistic effects than single metal hydroxides [26,27]. Therefore, in the present work, a facile ultrasound-assisted one-step fabrication of CoNi double hydroxide (UA-CoNi DH) microspheres at room

* Corresponding authors at: College of Chemistry and Materials Engineering, Zhejiang A&F University, Hangzhou 311300, China.
** Corresponding author.
E-mail addresses: yjpang@zafu.edu.cn (Y. Pang), iamcguan@nwpu.edu.cn (C. Guan), haochen@zafu.edu.cn (H. Chen).
[1] These authors contributed equally to this work.

https://doi.org/10.1016/j.cclet.2022.107768
1001-8417/

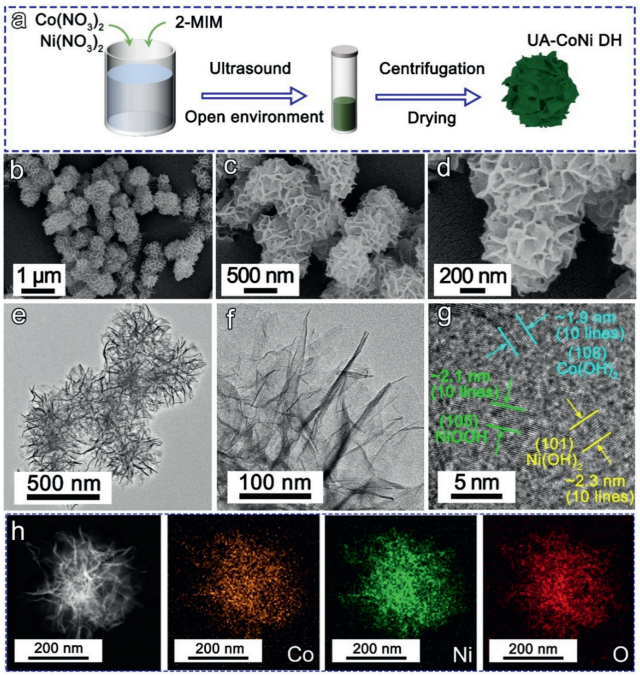

Fig. 1. (a) Schematic diagram of the synthetic route of UA-CoNi DH microspheres. (b-d) SEM images under various magnifications. (e-g) TEM and HRTEM images of the UA-CoNi DH microspheres under different magnifications. (h) The HAADF-STEM image and relative elemental distribution of the UA-CoNi DH microspheres.

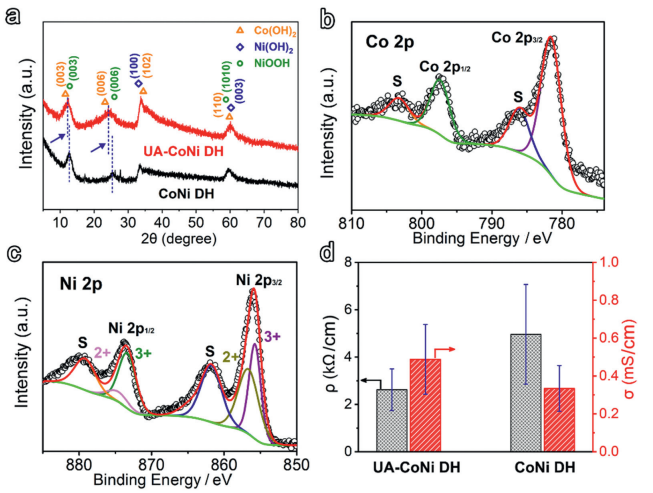

Fig. 2. (a) XRD patterns of CoNi DH and UA-CoNi DH. XPS spectrum of (b) Co 2p and (c) Ni 2p of UA-CoNi DH at high resolution. (d) Resistivity and conductivity of CoNi DH and UA-CoNi DH.

temperature is proposed, which displays a pronounced increase in Ni–Zn battery performance, including capacity and rate capability. Such an ultrasound-assisted method allows for the fabrication of metal double hydroxide micro-nano architecture with expanded interlayer spacing and improved conductivity, leading to a significantly enhanced electrochemical performance. In detail, the UA-CoNi DH as the electrode material exhibits greatly improved electrochemical activity relative to CoNi DH prepared without ultrasound assistance. Thanks to the enhanced performance of the UA-CoNi DH electrode, the aqueous Ni–Zn battery with UA-CoNi DH as the cathode (UA-CoNi DH//Zn) achieves an excellent specific capacity (202.36 mAh/g) and rate performance (70.49% retention at a 10-time increase in current), presenting more than 71.61% and 21.99% improvement relative to the CoNi DH//Zn battery, respectively.

Fig. 1a shows the production procedure for the UA-CoNi DH microspheres, which was fabricated using a one-step ultrasound-assisted approach that took advantage of the facile hydrolysis of Co^{2+} and Ni^{2+} in a 2-methylimidazole (2-MIM) solution. Specifically, $Co(NO_3)_2$, $Ni(NO_3)_2$, and 2-MIM were simply dissolved in a mixed solution of ethanol and water and then transferred to an ultrasonic disperser for 30 min of sonication at room temperature to complete the preparation. To get UA-CoNi DH, the product was then removed, centrifuged, and dried. Details on synthesis are given in the Experimental section (Supporting information). The foregoing reaction can be carried out because 2-MIM has weak basicity, allowing Co^{2+} and Ni^{2+} to bind with OH^- and produces $Co(OH)_2$, $Ni(OH)_2$, and NiOOH with the assistance of ultrasound. The UA-CoNi DH product is continually formed as the reaction advances, generating a microsphere shape. The scanning electron microscope (SEM) images of UA-CoNi DH reveal a regular microsphere structure with uniform nanosheets distributed on the surface (Figs. 1b–d). Although CoNi DH prepared without ultrasound assistance has a similar structure, it is less uniform (Fig. S1 in Supporting information). As further shown by transmission electron microscopy (TEM) images, the UA-CoNi DH spheres with a diameter of around 500 nm are independent of one another, and the numerous ultrathin nanosheets with a thickness of about 10 nm are equally dispersed on the surface of the spheres (Figs. 1e and f). Such a micro-nano architecture can largely facilize the electrochemical behavior during the redox reaction. Furthermore, the lattice fringes of different orientations and sizes are observed in the high-resolution TEM (HRTEM) image, revealing the polycrystalline nature of UA-CoNi DH (Fig. 1g). Among them, the lattice spacing of 0.19 nm corresponds to the $Co(OH)_2$ phase (JCPDS No. 46–0605), 0.21 nm corresponds to the NiOOH phase (JCPDS No. 06–0075), and 0.23 nm corresponds to $Ni(OH)_2$ phase (JCPDS No. 14–0117), respectively [17,28,29]. The presence of Co, Ni and O elements, as well as their homogenous distribution throughout the whole region viewed by the high-angle annular dark field-scanning transmission electron microscope (HAADF-STEM), can be seen in the energy-dispersive X-ray spectroscopy (EDS) mapping results (Fig. 1h).

Furthermore, the crystalline phases of both the synthesized UA-CoNi DH and CoNi DH products are identified using X-ray diffraction spectroscopy (XRD) as the combined diffraction signal of the $Co(OH)_2$ phase, $Ni(OH)_2$ phase, and NiOOH phase (Fig. 2a) [30–32], which agrees well with the above TEM results. Of note, a left shift is observed when comparing the positions of the detailed characteristic peaks, including (003) and (006) peaks noted in Fig. 2a. This shows that our designed one-step ultrasound-assisted technique expands the interlayer spacing of UA-CoNi DH, which might be related to acoustic cavitation generated by the creation, development, and implosive collapse of bubbles in the liquid owing to ultrasonic shearing [33]. After that, X-ray photoelectron spectroscopy (XPS) verifies that the surface of our UA-CoNi DH is composed of the expected elements, *i.e.*, including Co, Ni, O, and C (Fig. S2 in Supporting information). By further investigating the high-resolution XPS spectrum of Co 2p, one can see that the two peaks at 797.8 and 781.3 eV, respectively, are complemented by a neighboring satellite peak (marked as "S"), which corresponds to Co $2p_{1/2}$ and Co $2p_{3/2}$ of Co^{2+}, respectively. This indicates the +2 valence state of Co in our UA-CoNi DH (Fig. 2b). In contrast to this, by dividing the peaks in the high-resolution XPS spectrum of Ni 2p, we can obtain characteristic peaks belonging to the +2 valence and +3 valence states of Ni. The peaks located at 855.2 and 872.7 eV correspond to Ni^{3+}, while the other pair of peaks at 856.1 and 878.2 eV correspond to Ni^{2+} (Fig. 2c). This result demonstrates that part of Ni^{2+} can be oxidized to Ni^{3+}, yielding $Ni(OH)_2$

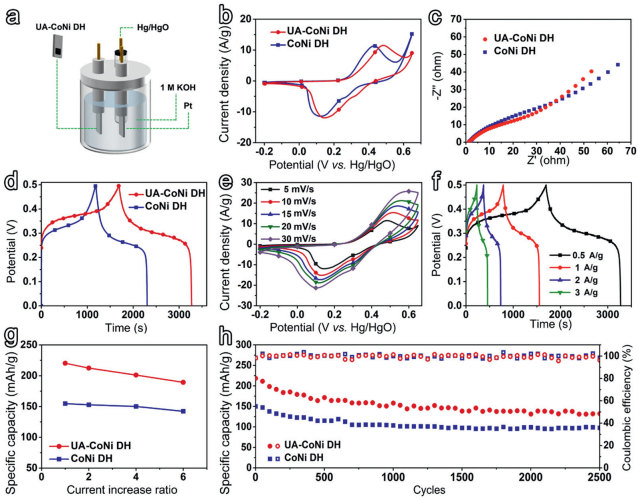

Fig. 3. (a) Schematic diagram of the test installation on a three-electrode system. Comparison of (b) CV curves at 5 mV/s, (c) Nyquist curves, (d) CD curves at 0.5 A/g, (g) specific capacities, and (h) cycling performance at 0.5 A/g between CoNi DH and UA-CoNi DH electrodes. (e) CV curves at different scan speeds, (f) CD curves at different current densities of the UA-CoNi DH electrode.

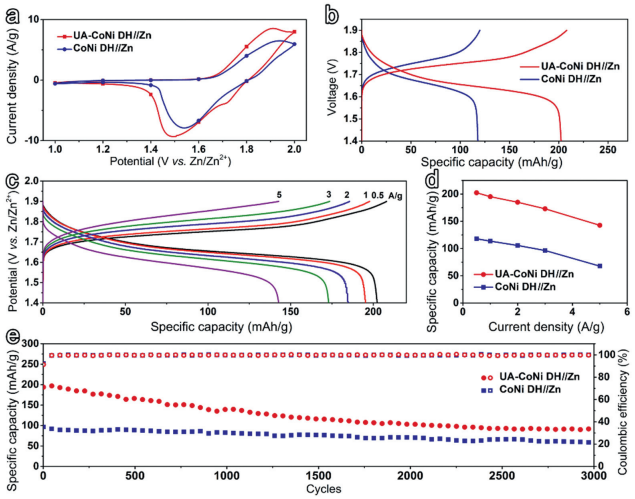

Fig. 4. Comparison of (a) CV curves, (b) CD curves, (d) rate performance, and (e) cycle performance at 5 A/g between CoNi DH//Zn and UA-CoNi DH//Zn batteries. (c) GCD curves of UA-CoNi DH//Zn at various current densities.

and NiOOH as a consequence. In addition, Fig. S3 (Supporting information) presents the existence form of O elements, including metal hydroxides (M-OH) and metal oxide (M-O). Therefore, by combining these above-mentioned results from systematic characterization and analysis, one can conclude that such an ultrasound-assisted one-step fabrication method can successfully induce the formation of metal hydroxide microspheres composed of NiOOH, $Ni(OH)_2$, and $Co(OH)_2$, as well as exhibiting enlarged interlayer spacing, thereby providing the opportunity to improve the electrochemical activity.

Prior to determining the electrochemical performance, the conductivity feature of our UA-CoNi DH was first investigated, and the results are shown in Fig. 2d, where UA-CoNi DH has a lower resistivity and better bulk conductivity than CoNi DH, which is therefore conducive to exerting its electrochemical activity as an electrode. The powder sample was subsequent evenly ground with conductive acetylene black and coated on the cleaned nickel foam surface to make an electrode, which was then employed as a working electrode in a utilized three-electrode test system (Fig. 3a). A pair of symmetric redox peaks from both CoNi DH and UA-CoNi DH electrodes observed in the cyclic voltammetry (CV) curves reveals good reversibility (Fig. 3b). Because their chemical and crystal compositions are comparable, the UA-CoNi DH preserves the same CV shape as the CoNi DH, indicating that their electrochemical processes are similar. The area difference of the region covered by the CV curve, on the other hand, implies that UA-CoNi DH has better electrochemical activity. Moreover, the intercept of the *X*-axis for UA-CoNi DH is smaller than that for CoNi DH in the high-frequency area of Nyquist curves, indicating a lower bulk resistance (Fig. 3c and Fig. S4 in Supporting information). The radius of the semicircle of UA-CoNi DH is likewise less than that of CoNi DH, implying that UA-CoNi DH has a lower charge transfer resistance. Moreover, in the low-frequency range, the line of the UA-CoNi DH electrode has a greater slope, indicating that it has a lower ionic diffusion resistance than the CoNi DH electrode [34]. Thanks to the improved electrochemical activity and smaller electrochemical resistance, the charge-discharge (CD) time of UA-CoNi DH is thus significantly prolonged, manifesting the enhanced electric charge storage capacity (Fig. 3d). Afterward, the CV curves of UA-CoNi DH at various scan speeds were examined (Fig. 3e). All CV curves are symmetrical, and when the sweep rate rises from 5 mV/s to 30 mV/s, the currents steadily increase, exhibiting acceptable electrochemical kinetics. The very symmetrical CD curves in Fig. S5 (Supporting information) and Fig. 3f also confirm this point.

The specific capacities under various current intensities were calculated using their CD curves and shown in Fig. 3g. The capacity of the UA-CoNi DH is much higher than that of the CoNi DH at all current densities evaluated. Furthermore, the rate capability of UA-CoNi DH outperforms that of CoNi-DH. And in a long-term test, our UA-CoNi DH also shows good cycle life with high Coulombic efficiencies (Fig. 3h).

A UA-CoNi DH//Zn aqueous battery was created utilizing Zn foil as the anode to further demonstrate the possible applicability of the UA-CoNi DH electrode as the cathode for Ni–Zn batteries. At a scan rate of 10 mV/s, the CV profiles of CoNi DH//Zn and UA-CoNi DH//Zn batteries are compared (Fig. 4a), where the distinct CV peaks are signs of the electrochemical reaction from Ni–Zn batteries, as demonstrated in previous studies [17,28]. The UA-CoNi DH//Zn battery achieves a high current density, as predicted, exhibiting its greater capacity due to larger interlayer spacing and improved chemical reactivity. Fig. 4b shows the typical voltage–capacity curves of UA-CoNi DH//Zn and CoNi DH//Zn batteries within the 1.4–1.9 V range at a given current density of 0.5 A/g, in which the specific capacity of UA-CoNi DH//Zn battery (202.36 mAh/g) is increased by 71.61% than that of CoNi DH//Zn battery (117.91 mAh/g). The performance is significantly improved, and it is also comparable to some of the reported literature [35,36]. Following that, according to the specific capacity at different current densities in Fig. S6 (Supporting information) and Fig. 4c, we can see that the capacity decreases with increasing charging current, which is consistent with the findings in the literature [37]. Moreover, the maximum energy and power density of our UA-CoNi DH//Zn battery are accepted relative to previous literature (Table S1 in Supporting information). And the capacity retention of two assembled CoNi DH//Zn and UA-CoNi DH//Zn batteries can be obtained, reaching 57.47% and 70.48%, respectively, with a 10-fold increase in current density (Fig. 4d). Evidently, benefitting from its lower surface ion diffusion resistance, our UA-CoNi DH//Zn battery exhibits enhanced rate performance. The long-term CD method was also used to examine the cycling durability of the two constructed batteries (Fig. 4e). It is noteworthy that although there is no significant improvement in durability, probably due to the conversion of more α-CoNi DH phases to β phases during charge/discharge processes of the UA-CoNi DH material with an expanded interlayer spacing [38], the UA-CoNi DH//Zn battery's specific capacity after the

long-term test is still higher that of the CoNi DH//Zn battery and even comparable to its initial capacity, demonstrating its superior capacity output.

In summary, a facile and efficient ultrasound-assisted one-step fabrication method has been verified to construct high-performance CoNi hydroxides (UA-CoNi DH). This ultrasound-assisted method can give rise to an elevation of interlayer spacing and conductivity of metal hydroxides, as demonstrated by the experimental results, relative to the CoNi DH electrode prepared without ultrasound assistance. Consequently, the as-obtained UA-CoNi DH as the electrode material displays considerably increased electrochemical performance and attains a high specific capacity (202.36 mAh/g) and good rate capability (70.49% retention at a 10-fold higher current) when severing as a cathode in the assembled aqueous Ni–Zn battery (UA-CoNi DH//Zn), which displays more than 71.61% and 21.99% improvement respectively relative to the CoNi DH//Zn battery. This study not only supplies a new-fashioned ultrasound-assisted strategy but offers a fresh reference and enlightenment for synthesizing advanced electrodes for high-performance Ni–Zn batteries.

Declaration of competing interest

The authors declare that they have no known competing financial interests or personal relationships that could have appeared to influence the work reported in this paper.

Acknowledgments

The authors thank the supports from the Zhejiang Provincial Natural Science Foundation of China (No. LQ22B060003), the Fundamental Research Funds for the Provincial Universities of Zhejiang (No. 2020YQ005), Zhejiang Provincial Key Research and Development Project (No. 2019C02037), China Postdoctoral Science Foundation (No. 2019M662044), Research Foundation of Talented Scholars of Zhejiang A&F University (Nos. 2020FR069, 2022LFR024, 2022LFR025), National-Level College Students Innovative Entrepreneurial Training Program of Zhejiang A&F University (No. 202101341031), and 151 Talent Project of Zhejiang Province.

Supplementary materials

Supplementary material associated with this article can be found, in the online version, at doi:10.1016/j.cclet.2022.107768.

References

[1] X. Cheng, Z. Shen, L. Jiao, et al., EnergyChem 3 (2021) 100066.
[2] D. Chao, W. Zhou, F. Xie, et al., Sci. Adv. 6 (2020) eaba4098.
[3] Y. Cheng, H. Wang, T. Qian, et al., EnergyChem 4 (2022) 100074.
[4] L. Li, W. Liu, H. Dong, et al., Adv. Mater. 33 (2021) 2004959.
[5] W. He, W. Guo, H. Wu, et al., Adv. Mater. 33 (2021) 2005937.
[6] M. Han, J. Yao, J. Huang, et al., Chin. Chem. Lett. 34 (2023) 107493.
[7] J. Pu, Y. Gao, Q. Cao, et al., SmartMat 3 (2022) 608–618.
[8] M. Han, L. Qin, Z. Liu, et al., Mater. Today Energy 20 (2021) 100626.
[9] S. Zheng, Y. Sun, H. Xue, et al., Natl. Sci. Rev. (2021) nwab197.
[10] P. Geng, L. Wang, M. Du, et al., Adv. Mater. 34 (2022) 2107836.
[11] P. Ruan, S. Liang, B. Lu, H.J. Fan, J. Zhou, Angew. Chem. Int. Ed. 61 (2022) e202200598.
[12] C. Xie, Q. Zhang, Z. Yang, et al., Chin. Chem. Lett. 33 (2022) 2653–2657.
[13] J. Jiang, J. Liu, Interdiscip. Mater. 1 (2022) 116–139.
[14] Z. You, W. Hua, N. Li, H. Liu, J.G. Wang, Chin. Chem. Lett. 34 (2023) 107525.
[15] J. Tan, J. Liu, Energy Environ. Mater. 4 (2021) 302–306.
[16] Y. Yu, J. Xie, H. Zhang, et al., Small Sci. 1 (2021) 2000066.
[17] Y. Pang, L. Li, Y. Wang, et al., Chem. Eng. J. 436 (2022) 135202.
[18] Y. Shen, K. Zhang, F. Yang, et al., Sci. China Mater. 63 (2020) 1205–1215.
[19] Q. Liu, X. Zhao, X. Yang, Chin. Chem. Lett. 33 (2022) 2648–2652.
[20] W.Y. Zhao, Z.Q. Liu, C.L. Zhong, et al., J. Colloid Interface Sci. 579 (2020) 823–831.
[21] N. Kamboj, R.S. Dey, J. Power Sources 512 (2021) 230527.
[22] Y. Zeng, Y. Meng, Z. Lai, et al., Adv. Mater. 29 (2017) 1702698.
[23] Z. Peng, C. Yang, Q. Zhao, et al., J. Colloid Interface Sci. 607 (2022) 61–67.
[24] Y. Zhou, X. Tong, N. Pang, et al., ACS Appl. Mater. Interfaces 13 (2021) 34292–34300.
[25] R. Wang, Y. Han, Z. Wang, et al., Adv. Funct. Mater. 28 (2018) 1802157.
[26] H. Chen, Z. Shen, Z. Pan, et al., Adv. Sci. 6 (2019) 1802002.
[27] Y. Wu, H. Chen, Y. Lu, et al., J. Colloid Interface Sci. 581 (2021) 455–464.
[28] X. Zhu, Y. Wu, Y. Lu, et al., J. Colloid Interface Sci. 587 (2021) 693–702.
[29] K. Li, B. Zhao, J. Bai, et al., Small 16 (2020) 2001974.
[30] J. Ning, M. Xia, D. Wang, et al., Nano-Micro Lett. 13 (2020) 2.
[31] K. Li, M. Liu, S. Li, et al., J. Alloys Compd. 817 (2020) 152712.
[32] W.S. Li, M.L. Chang, H.C. Cheng, Chem. Phys. Lett. 739 (2020) 137003.
[33] W. Zhao, P. Yan, H. Yang, et al., Nat. Synth. 1 (2022) 87–95.
[34] C. Guan, X. Liu, W. Ren, et al., Adv. Energy Mater. 7 (2017) 1602391.
[35] S. Wang, X. Duan, T. Gao, et al., J. Electrochem. Soc. 167 (2020) 160550.
[36] X. Xuan, M. Qian, L. Pan, et al., J. Energy Chem. 70 (2022) 593–603.
[37] J. Partridge, D.I. Abouelamaimen, Energies 12 (2019) 2683.
[38] Q. Pan, F. Zheng, D. Deng, B. Chen, Y. Wang, ACS Appl. Mater. Interfaces 13 (2021) 56692–56703.